11th World Congress on Computational Mechanics (WCCM XI)
5th European Conference on Computational Mechanics (ECCM V)
6th European Conference on Computational Fluid Dynamics (ECFD VI)
E. Oñate, J. Oliver and A. Huerta (Eds)

COMPUTATIONAL ASSESSMENT OF REDUCTION METHODS IN FE-BASED FREQUENCY-RESPONSE ANALYSIS

Frank Ihlenburg*, Robert Möllenhoff†, and Martin Wandel††

*University of Applied Sciences Hamburg
Berliner Tor 21, D-20099 Hamburg, Germany
e-mail: frank.ihlenburg@haw-hamburg.de, web page: http://www.mp.haw-hamburg.de/

†Volkswagen Motorsport Braunschweig

††Airbus Hamburg

Key words: Structural Dynamics, Finite-Element Method, Frequency Response, Reduced-Order Methods

Abstract. State-of-the art FE solvers offer several methods for dimensional reduction of the matrices, including the traditional method of Component Mode Substructuring (CMS) and the more recent approach of Automated Multilevel Substructuring (AMLS). All reduction methods are associated with specific rectangular transformation matrices $\mathbf{T}$. Those matrices represent the basis of a subspace onto which the full frequency response analysis is projected. The subspaces are usually based on dynamic modes (eigenvectors) or static modes (Ritz vectors), or a combination of both. From a mechanical viewpoint, the eigenmodes represent the inherent dynamic features of the structure while the static modes capture the action of the applied load. We give a short overview of several dimensional reduction and modal enrichment approaches, and discuss computational results for a medium-scale model problem and a large-scale industrial application.

1 Introduction

The frequency response of thin-walled structures to dynamic loads is of major practical interest in light-weight constructions such as cars, airplanes or space structures. In early stages of the design process, only a computational investigation of the frequency response is possible due to the lack of prototypes. Clearly, the computational methods for frequency response analysis (FRA) should be both efficient and reliable. In this paper we compare several methods for computational FRA. The investigation was carried out in an industrial environment, using a commercial solver. We have used FE-models of typical fuselage

structures. We first consider a broad-band FRA on a downsized, medium-scale model with about 600k DOF. Then we turn to a true-scale model with about 2m DOF.

The paper is organised as follows: section 2 contains a brief review of computational methods for FE-based FRA, with an emphasis on reduced-order methods. The efficiency and reliability of the methods is discussed from a theoretical viewpoint in Section 3, and computational results are surveyed in Section 4.

2 Methods

The finite element equations of linear structural dynamics have the form

$$\mathbf{M}\ddot{X} + \mathbf{D}\dot{X} + \mathbf{K}X = P\,, \tag{2.1}$$

with the typical notations for the mass, damping, and stiffness matrices. The stationary solutions for time-harmonic excitations with a driving frequency Ω and a complex-valued force amplitude p can be computed in the frequency range by solving

$$\left[\mathbf{K} + \mathrm{i}\Omega\mathbf{D} - \Omega^2\mathbf{M}\right] u = p\,. \tag{2.2}$$

The system can be written in the form $\mathbf{K}(\Omega)u = p$ with the dynamic stiffness matrix $K(\Omega) = \mathbf{K} + \mathrm{i}\Omega\mathbf{D} - \Omega^2\mathbf{M}$. In practice, the solution is usually required in a frequency band $\Omega \in [\Omega_{\min}, \Omega_{\max}]$.

If the matrix dimension N is small, or the response is computed just for a few driving frequencies, it is usually best to build $\mathbf{K}(\Omega)$ for every driving frequency in the band and to solve eq. (2.2) with a direct frontal solver. This is equivalent to inverting the dynamic stiffness matrix, or $u(\Omega) = \mathbf{H}(\Omega)p$ with the transfer matrix $\mathbf{H}(\Omega) = \mathbf{K}^{-1}(\Omega)$. Since the direct approach can be very costly for large-scale simulations in broad frequency bands, dimensional reduction may be advised. The reduced system can be written in the form

$$\left[\tilde{\mathbf{K}} + \mathrm{i}\Omega\tilde{\mathbf{D}} - \Omega^2\tilde{\mathbf{M}}\right] q = \tilde{p}\,, \tag{2.3}$$

where the matrices $\tilde{\mathbf{K}} = \mathbf{T}^T\mathbf{K}\mathbf{T}$ etc. are obtained from a transformation with a rectangular reduction matrix $\mathbf{T}$ of dimension $N \times k$ with $k \ll N$. The overall computational effort of the reduced method then involves the computation of the reduction matrix $\mathbf{T}$, the dimensional reduction itself, and the solution of the reduced system, where usually the computation of the reduction matrix is the most costly step. Solving the linear system (2.3) for q is equivalent to finding a reduced transfer matrix $H_k(\Omega)$.

Modal Reduction

If the exact solution is approximated by a linear superposition of eigenmodes

$$u \approx u_k = \sum_{j=1}^{k} q_j x_j\,, \tag{2.4}$$

the reduction matrix

$$\mathbf{T}_{MR} = X_k = [x_1, \ldots, x_k] \tag{2.5}$$

is the rectangular matrix containing the eigenvektors x_j, which are computed from the linear (undamped) eigenproblem

$$\left[\mathbf{K} - \omega^2 \mathbf{M}\right] x = 0\,. \tag{2.6}$$

If $\mathbf{K}$ and $\mathbf{M}$ are symmetric, the eigenvectors are real-valued and orthogonal. Assuming that the vector set X_k is mass-orthonormalized, i.e. $X_k^T \mathbf{M} X_k = \mathbf{I}$, the reduced stiffness is $\tilde{\mathbf{K}} = diag\,(\omega_1^2, \ldots, \omega_k^2) := \mathbf{\Lambda}$. If the damping matrix is proportional to the stiffness matrix, or a superposition of mass and stiffness matrices, then the reduced dynamic stiffness matrix and the transfer matrix $\mathbf{H}_k$ are also diagonal. The reduced linear system (2.3) thus decouples into k independent equations, yielding scalar transfer functions $H_j(\Omega), j = 1, \ldots, k$. Obviously $\mathbf{T}$ defines a congruence transformation if $k = N$, i.e. all N eigenvectors are included. A dimensionally reduced system is obtained by selecting $k \ll N$.

Static (Guyan) Reduction

Writing the stiffness matrix (after reordering) in the block-diagonal form

$$\mathbf{K} = \begin{bmatrix} K_{aa} & K_{ap} \\ K_{pa} & K_{pp} \end{bmatrix}$$

with square matrices K_{aa} and K_{pp} of dimensions m and $n = N - m$, respectively, we can compute the Guyan matrix $G = -K_{pp}^{-1} K_{pa}$ and define the reduction matrix

$$\mathbf{T}_G = \begin{bmatrix} I_{n\times n} \\ G_{m\times n} \end{bmatrix} \tag{2.7}$$

of so-called static modes. This reduction matrix can be applied either to the forced-vibration equation 2.2 or to the eigenvalue problem 2.6.

Static-dynamic Reduction (Component Mode Synthesis)

Guyan reduction decomposes the original structure into two substructures, containing active nodes (or rather, DOFs) "a" and passive or dependent DOFs "p". The static mode shapes are associated with the active DOFs only. This statically reduced basis can be enriched by dynamic mode shapes to obtain the transformation matrix

$$\mathbf{T}_{CMS} = \begin{bmatrix} I_{n\times n} & 0 \\ G_{m\times n} & X_{m\times k} \end{bmatrix}, \tag{2.8}$$

where the submatrix X contains eigenmodes of the passive substructures, with all active DOFs fully constrained. This approach is called Component Mode Synthesis (CMS). The transformation matrix can be factorised as $\mathbf{T} = \mathbf{LR}$, with

$$\mathbf{L} = \begin{bmatrix} I & 0 \\ G & I \end{bmatrix}, \qquad \mathbf{R} = \begin{bmatrix} I & 0 \\ 0 & X \end{bmatrix},$$

where $\mathbf{L}$ is a lower triangular, block-Gaussian elimination matrix and $\mathbf{R}$ represents the modal reduction of the dependent substructure. The reduced original stiffness and mass matrices have the form

$$\tilde{\mathbf{K}} = \begin{bmatrix} \tilde{K}_{ss} & 0 \\ 0 & \omega^2 \end{bmatrix}, \qquad \tilde{\mathbf{M}} = \begin{bmatrix} \tilde{M}_{ss} & \tilde{M}_{sd} \\ \tilde{M}_{ds} & I \end{bmatrix},$$

where $\tilde{K}_{ss}$ and $\tilde{M}_{ss}$ are the statically (Guyan-) reduced submatrices, ω is a diagonal matrix of eigenmodes, and $\tilde{M}_{ds} = \tilde{M}_{sd}^T$ is a fully populated, "static-dynamic" rectangular submatrix.

The transformation can be further reduced by solving the generalised eigenproblem for the stencil $\left(\tilde{K}_{ss},\, \tilde{M}_{ss}\right)$, to obtain a set $X_{n\times r}$ of eigenvectors. Setting $\mathbf{T} = \mathbf{LR}$, with

$$\mathbf{R} = \begin{bmatrix} X_{n\times r} & 0 \\ 0 & X_{m\times k} \end{bmatrix}, \tag{2.9}$$

then yields reduced matrices of dimension $k + r$.

Automated Multilevel Substructuring

The CMS was generalised to an automated multilevel approach by Bennighoff [2]; see also [3, 10, 19]. In this approach, the original domain (or the set of unconstrained DOF) is subdivided into l_1 subdomains (or subsets). The first-level subdomains are further partitioned further into l_{2j} domains etc., down to some level s. If $l \equiv 2$ on all levels, the substructuring can be represented by a binary tree as shown in Fig. 1.

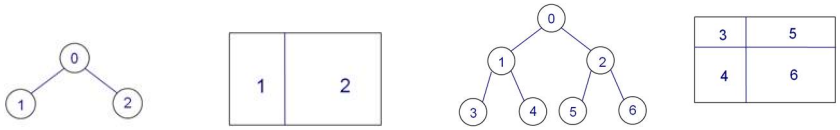

Figure 1: Domain decomposition and corresponding binary tree for one level (left) and two levels (right)

The stiffness and mass matrices are reordered in accordance with the substructuring. For example, the one-level approach leads to

$$\mathbf{K} = \begin{bmatrix} K_{00} & K_{01} & K_{02} \\ K_{00}^T & K_{11} & 0 \\ K_{02}^T & 0 & K_{22} \end{bmatrix} \qquad \mathbf{M} = \begin{bmatrix} M_{00} & M_{01} & M_{02} \\ M_{01}^T & M_{11} & 0 \\ M_{02}^T & 0 & M_{22} \end{bmatrix},$$

where the block-matrix K_{00} corresponds to the active DOF on the original domain, the matrices K_{11} and K_{22} correspond to the passive DOF on the subdomains 1 and 2, and the off-diagonal entries are coupling matrices. The CMS transformation can then be expressed by the matrix operator

$$\mathbf{T} = \begin{bmatrix} I_n & 0 & 0 \\ G_{m_1 \times n} & X_{m_1 \times k_1} & 0 \\ G_{m_2 \times n} & 0 & X_{m_2 \times k_2} \end{bmatrix}$$

with $n + m_1 + m_2 = N$, where n, m_1, m_2 denote the numbers of active and passive DOF, respectively, and k_1 and k_2 the numbers of modal DOF on the subdomains. As shown with the transformation (2.9), the matrix size can be further reduced by computing a number of k_{01} eigenmodes for the stencil (K_{00}, M_{00}) and replacing the identity matrix with a modal matrix $X_{n \times k_0}$.

Similarly, for the two-level approach the reordered stiffness matrix has the form

$$\mathbf{K} = \begin{bmatrix} K_{00} & K_{01} & K_{02} & K_{03} & K_{04} & K_{05} & K_{06} \\ K_{01}^T & K_{11} & & K_{13} & K_{14} & & \\ K_{02}^T & & K_{22} & & & K_{25} & K_{26} \\ K_{03}^T & K_{13}^T & & K_{33} & & & \\ K_{04}^T & K_{14}^T & & & K_{44} & & \\ K_{05}^T & & K_{25}^T & & & K_{55} & \\ K_{06}^T & & K_{26}^T & & & & K_{66} \end{bmatrix},$$

where the diagonal entries correspond to DOF that are:

K_{00}**:** active on the first level (the original domain),

K_{11}, K_{22}**:** passive on the first but active on the second level (in subdomains 1 and 2),

$K_{33} - K_{66}$**:** passive on the second (here: the lowest) level,

and $K_{ij}, i \neq j$ are coupling matrices.

The operator of the two-level CMS transformation can now again be written as a product $\mathbf{T} = \mathbf{LR}$, where now

$$\mathbf{L} = \begin{bmatrix} I & & & & & & \\ G_{01} & I & & & & & \\ G_{02} & & I & & & & \\ G_{03} & G_{13}^T & & I & & & \\ G_{04} & G_{14}^T & & & I & & \\ G_{05} & & G_{25}^T & & & I & \\ G_{06} & & G_{26}^T & & & & I \end{bmatrix}, \quad \mathbf{R} = \begin{bmatrix} X_0 & & & & & & \\ & X_1 & & & & & \\ & & X_2 & & & & \\ & & & X_3 & & & \\ & & & & X_4 & & \\ & & & & & X_5 & \\ & & & & & & X_6 \end{bmatrix}. \quad (2.10)$$

Ritz Vectors and Residual Vectors

The eigenmodes represent inherent dynamical properties of a structure but they are not related to the mechanism of excitation. Based on this observation, Wilson [20] proposed to construct an alternative basis of so-called Ritz vectors by the following algorithm: Given a "static distribution of the dynamic loading" p, compute

$$\begin{aligned} &\text{START}(i=1): \qquad Ky = p \qquad \rightarrow \qquad y = K^{-1}p \qquad \rightarrow \qquad y_1 = \frac{y}{\sqrt{y^T M y}} \\ &i = 2, \ldots, k: \quad Ky = My_{i-1} \quad \rightarrow \quad y^* = y - \sum_{j=1}^{i-1} \left(y_j^T M y\right)\, y_j \quad \rightarrow \quad y_i = \frac{y^*}{\sqrt{(y^*)^T\, M y^*}}\,. \end{aligned} \tag{2.11}$$

This algorithm starts from the static solution; i.e. the "displacement vector obtained from a static analysis" of the problem. New vectors are then computed in subsequential steps, each of which involves an orthogonalisation w.r. to all former base vectors. The k Ritz vectors are then assembled in the projection matrix $\mathbf{T} = [y_1, \ldots, y_k]$ and used for model reduction to a system size $k \times k$.

Dickens [9] proposed to use Ritz vectors in combination with eigenmodes to enrich the basis of standard modal reduction. The Ritz vectors are computed not for the original load p but for the residual load

$$r_k = \mathbf{K}(\Omega) e_k = p - \mathbf{K}(\Omega) u_k, \tag{2.12}$$

where $e_k = u - u_k$ is the truncation error of modal projection. The approximation u_k lies in the subspace V_k spanned by the eigenvectors $x_1, \ldots, x_k$. Since all N eigenvectors form an orthonormal base of the full space, we have $V_N = V_k \oplus V_r$ with the residual subspace $V_r = \text{span}\,\{x_{k+1}, \ldots, x_N\}$. If the modal transformation diagonalises the dynamic stiffness matrix $K(\Omega)$ then $e_k \in V_r$ implies $r_k \in V_r$, and it can be shown [9] that

$$r_k = \left[\mathbf{I} - \mathbf{M} X_k X_k^T\right]\, p\,. \tag{2.13}$$

Based on this relation, one can efficiently compute a set $\{r_{k,j}\}$ of residual load vectors for all non-zero components p_j of the original load vector. The *residual vectors* are the corresponding static mode shapes $y_j = \mathbf{K}^{-1} r_{k,j}$. These vectors are then used to compute reduced stiffness and mass matrices $\hat{\mathbf{K}}, \hat{\mathbf{M}}$. An orthonormalised enrichment of the original basis is then finally obtained by solving the eigenproblem for the stencil $(\hat{\mathbf{K}}, \hat{\mathbf{M}})$. The algorithm can be summarized as follows,

$$\begin{aligned} &1) \quad \left[\mathbf{K} - \omega^2 \mathbf{M}\right] x = 0 \quad \rightarrow \quad \omega_, \ldots, \omega_k; \quad X_k = [x_1, \ldots, x_k] \\ &2) \quad p = \sum_{j=1}^{l} p_j \qquad\qquad \rightarrow \quad r_{k,j} = \left[I - \mathbf{M} X_k X_k^T\right] p_j \\ &3) \quad \mathbf{K} y_j = r_{k,j} \qquad\qquad \rightarrow \quad Y_l = [y_1, \ldots, y_l] \;\rightarrow\; \hat{\mathbf{K}} = Y_l^T \mathbf{K} Y_l,\; \hat{\mathbf{M}} = Y_l^T \mathbf{M} Y_l \\ &4) \quad \left[\hat{\mathbf{K}} - \omega^2 \hat{\mathbf{M}}\right] z = 0 \quad \rightarrow \quad Z_l = [z_1, \ldots, z_l] \;\rightarrow\; W = YZ\,, \end{aligned} \tag{2.14}$$

using the short notation p_j for the load vectors $[0, \ldots, p_j, \ldots]^T$. The enriched set $[X, W]$ of basis vectors is applied for modal reduction of the original frequency response equation $\mathbf{K}(\Omega)u = p$.

Krylov Subspace Methods

The recurrence algorithm for the computation of Ritz vectors was identified in [18] as a creation of a Krylov subspace basis; cf. also [6]. For a given matrix A and vector r, the Krylov subspace of order k is defined as

$$\mathcal{K}_k(A, r) = \left\{ r, Ar, \ldots, Ar^{k-1} \right\} .$$

In structural dynamics, the sequence is built with $r = K^{-1}p$ and $A = K^{-1}M$. The reduction operator T is obtained from $\mathcal{K}_k(A, r)$ by orthogonalisation, using, e.g., the Gram-Schmidt procedure [6] or the Arnoldi method [13, 4]. The Krylov subspace can be equivalently based on a set of linearly independent Lanczos vectors $q_1, \ldots, q_k$[1]. For FRA with proportional damping, the Krylov subspace approach can be related to a Taylor series expansion of the scalar transfer matrix $H_k(\Omega)$ around an arbitrary central frequency Ω_0 [1, 4], and it can be shown that the Krylov vectors generate the first $2k$ members of this expansion. The approximation error of the dimensional reduction is hence of the order $\mathcal{O}(\Omega - \Omega_0)^{2k}$ [1].

Fast FRA

We have pointed out that modal reduction is particularly efficient if the damping matrix is proportional to a superposition of mass and stiffness matrices. This global damping assumption cannot be always be upheld in practice. The equations for a linear dynamical system with non-proportional damping can be written in the form [15]

$$\left[(1 + i\theta)\mathbf{K} + \mathrm{i}K_{loc} + \mathrm{i}\Omega\mathbf{D} - \Omega^2\mathbf{M}\right] u = p \,, \tag{2.15}$$

where θ is the loss factor of a global material damping assumption, K_{loc} is a local structural damping matrix, and Matrix D represents (global and local) viscous damping effects. Modal reduction with k eigenvectors from the undamped stencil $(\mathbf{K}, \mathbf{M})$ will then lead to the reduced set of equations

$$\left[(1 + i\theta)\mathbf{\Lambda} + \mathrm{i}\tilde{K}_{\mathrm{loc}} + \mathrm{i}\Omega\tilde{\mathbf{D}} - \Omega^2\mathbf{I}\right] q = \tilde{p} \,, \tag{2.16}$$

in which the matrices $\tilde{\mathbf{K}}_{loc}$ and $\tilde{\mathbf{D}}$ are, in general, fully populated. Kim and Bennighof [15] propose an algorithm that involves a pseudo-diagonalisation of $\tilde{\mathbf{D}}$ by singular-value decomposition, and the diagonalisation of $(1+i\theta)\mathbf{\Lambda}+\tilde{K}_{loc}$ by a transformation with complex eigenvectors that are obtained from the solution of a complex symmetric eigenvalue problem. The r complex mode shapes are used for a second modal reduction of the reduced

system to the size $r \times r$. The reduced system matrix is the sum of two matrices, one of which is complex-diagonal and the other a product of low-rank matrices, including a pseudodiagonal matrix. This reduced matrix can be efficiently inverted using the ShermanMorrisonWoodbury formula [11, 2.1.3].

3 Efficiency and Reliability

Substructuring and Standard Modal Basis (Eigenvectors)

We have seen that CMS and AMLS transformations can be written as a product $\mathbf{T} = \mathbf{LR}$ of a congruence transform (on the original set of DOF) and modal reductions (on disjunct subdomains). The Guyan matrices G_{ij} in the operator $\mathbf{L}$ involve the inversion of block-matrices, and the modal matrices X_i in $\mathbf{R}$ require the solution of generalized eigenproblems (on subdomains). The overall numerical effort thus depends *superlinearly on the size of the subdomains*, but it depends only *linearly on the number of domains*. It is therefore favorable, from the numerical viewpoint, to subdivide the original domain into a large number of small-sized subdomains. Obviously care must be taken to assure that the modal bases on the subdomains are sufficiently rich to represent, together with the interface modes, the global structural dynamics in a frequency range of interest.

It is generally recommended to choose an upper frequency $\omega_{\max}$ of modal analysis such that the computed eigenspectrum $[\omega_1, \omega_k]$ exceeds the range $[\Omega_{\min}, \Omega_{\max}]$ of forcing frequencies. In practice this amounts to a rule of the form $\omega_{\max} = \alpha\Omega_{\max}$ with $\alpha > 1$. Since the lowest eigenfrequencies depend inversely on the size of the (sub)structures, the upper frequency bounds on the substructures should be higher than the global bound. This can be achieved by introducing additional, size-dependent "upfactors" β_{loc} and using the general rule with $\alpha_{loc} = \beta_{loc}\alpha$ on the subdomains.

Enriched Modal Basis (Residual Vectors)

The additional cost for the computation of residual vectors is theoretically balanced by the gain in quality of approximation. The combined basis of modal and residual vectors represents, from the mechanical viewpoint, the dynamic features both of the structure and of the force excitation. The overall cost may be even reduced in practice if the upper frequency bound in modal analysis can be lowered due to the enrichment by residual vectors. In the context of the domain decomposition approaches CMS and AMLS, the upscale factors β_{loc} on the subdomains can be reduced accordingly.

Alternative Modal Basis (Ritz and Krylov Vectors)

The first step of the algorithms involve the inversion of the satic stiffness matrix $\mathbf{K}$. The subsequent members of the Krylov base are computed by matrix-vector multiplication, which is computationally inexpensive. The orthogonalisation procedure is more time-consuming. It may be particularly advantageous to construct alternative modal bases

if their size, for the same error of approximation, can be chosen smaller than that of traditional modal bases.

Krylov subspace methods were applied to calculate the frequency response of thin-walled structures (car bodies) in [13]. An related Arnoldi method for model-order reduction of dynamical systems with non-symmetric stiffness matrices is proposed in [4] and applied to the FRA of machine tools. Different variants of Arnoldi algorithms are compared to the standard modal reduction approach. In most of the computational examples, the computational error of the Krylov methods is significantly lower than the corresponding error of FRA with modal reduction, with the same, or even smaller, dimension of the reduced system matrices.

4 Numerical Results

The reliability and efficiency of different reduction methods was assessed in computational experiments on two FE-models of typical thin-walled structures. We first consider the response of a medium-sized structure to a broad-band excitation and then proceed to a production case on a larger scale.

4.1 Medium-scale Model

The first series of computations was carried out on a simple thin-walled, cross-stiffened, structural model that is similar to two sections of a typical aircraft fuselage, but scaled down in size. The FE-model consists of about 90,000 shell and 6,000 beam elements, amounting to about 600,000 structural DOF. A detail of the computational model is depicted in Figure 2.

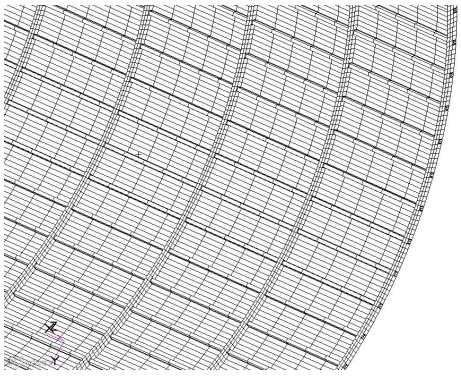

Figure 2: Small-scall computational model (detail)

The FRF curves have been calculated in several measuring points (FE-nodes). All curves will show the amplitude of normal displacement at one selected measuring point. The frequency response to a randomly distributed set of dynamic point forces was calculated. We have distributed the structural damping effects evenly across the model by

assigning the same loss factor (parameter GE in MSC/Nastran) to all material cards. The exact frequency response is obtained by direct solution of eq. (2.2). All calculations have been carried out with MSC/Nastran on a personal computer with 8 CPUs, a clock frequency of 5912MHz and 3317MB physical memory. The frequency response is in all cases computed from 10Hz to 1kHz in 1Hz steps.

Modal Reduction (MR)

Figure 3 shows the results of modal reduction with different upper frequency bounds. We can see that a factor $\alpha = 1.2$ yields satisfactory results for this particular structure. The option to choose a rather low factor is in this case related to the high modal density in the high-frequency end of $[\Omega_{\min}, \Omega_{\max}]$; see the first row in Table 1.

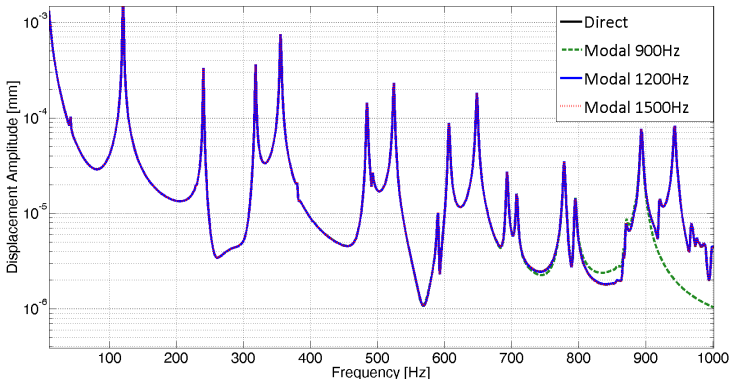

Figure 3: FRF: direct solution vs. modal reduction

Table 1: Computational effort: Modal reduction with different upper frequency bounds

Measure/ Method		MR/ Upper Frequency Limit			
	Direct	600Hz	900Hz	1.2kHz	1.5kHz
# of Modes		45	104	517	1,018
Sys. time (min)	176.46	0.39	0.88	6.58	10.87
Disk usage (MB)	5,436.13	3,984.22	4,801.06	9,316.03	17,557.50

Component Mode Synthesis (Superelement)

The performance of the CMS reduction, with the default settings for upscaling, is displayed in Table 2. The structure was subdivided into two geometrical subdomains (one "superelement" and one "residual structure") with about equal numbers of DOFs. The solver offers two alternative procedures. In the "internal" approach, the CMS is performed

within the frequency response run. In the "external" approach, the CMS-reduced matrices are precomputed and read from disk files during the frequency response solution. This explains the large difference in run time and disk usage between the two approaches. We remark that the "external" technology with CMS-reduced parts is frequently used in the coupling of FEM and MKS. The FRF graphs are identical for both CMS approaches, and in very good visual agreement with the direct solution, as can be seen from Figure 4

Table 2: Computational effort: direct solution vs. CMS

	Direct	CMS/int.	CMS/ext.	MR/1.2kHz
# of Modes		515	515	517
Sys. time (min)	176.46	28.46	2.50	6.58
Disk usage (MB)	5,436.13	58,945.54	5,998.47	9,316.03

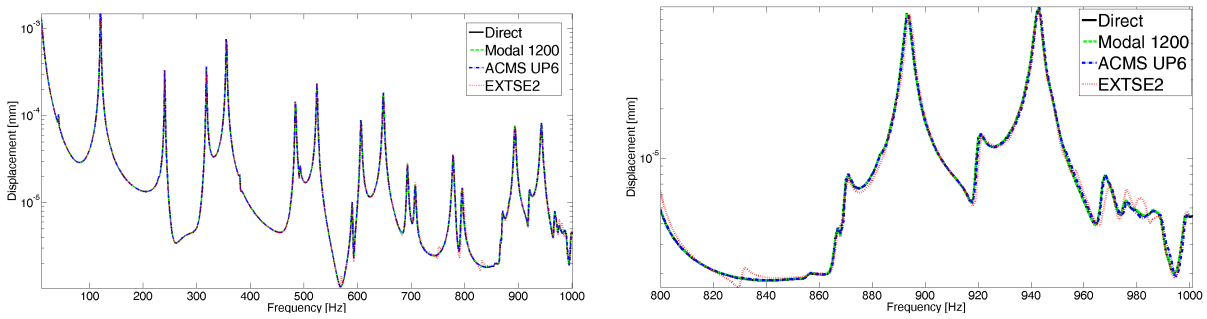

Figure 4: FRF: CMS compared to the direct method and modal reduction; upper frequency detail shown on the right.

Automated Component Mode Synthesis

We now turn to the investigation of AMLS (called ACMS in MSC/Nastran). Figure 5 shows the FRFs of the direct solution and the reduced method, using the default parameters of the solver for the latter. The corresponding comparison of numerical effort is displayed in Table 3.

Table 3: Computational effort: Direct solution ACMS (default settings) and MR

	Direct	ACMS	MR/1.2kHz
# of Modes		470	517
Sys. time (min)	176.46	0.62	6.58
Disk usage (MB)	5,436.13	5,320.63	9,316.03

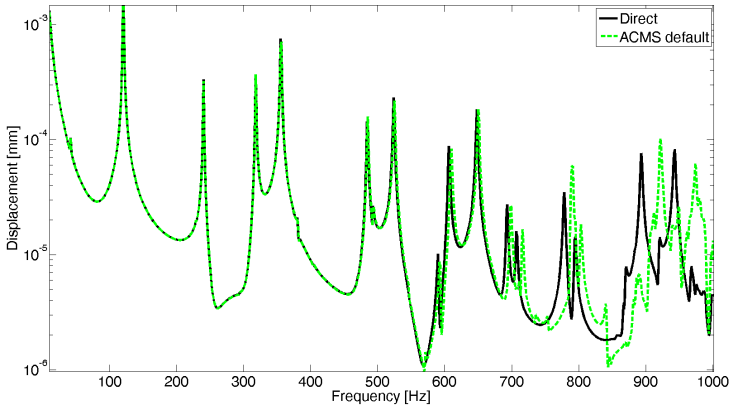

Figure 5: FRF: direct solution vs. domain decomposition (ACMS, default settings)

The influence of the number of subdomains is investigated in Figure 6 and in Table 4. The numbers in the column headings indicate the size of the lowest level of the binary tree. By increasing the number of subdomains, we gain in computational efficiency (as could be predicted from the theoretical considerations of the preceding section) but not in reliability. On the contrary, less modes are computed for the same upper frequency bound if the number of domains is increased.

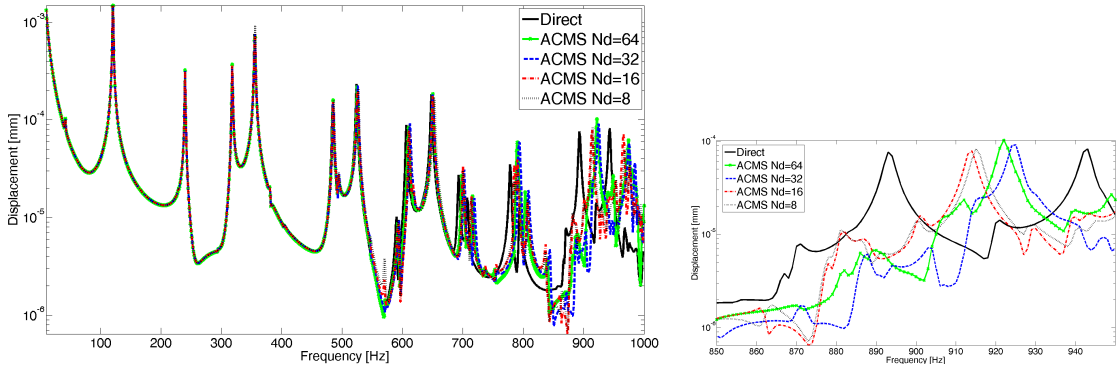

Figure 6: Domain decomposition: dependence on the number of subdomains

We now vary the local upper frequency bounds on the subdomains by increasing the "upscale" parameter β_{loc} from 2 (default) to 8, using each time $N = 64$ subdomains on the finest partition. The results are shown in Figure 7 and Table 5. We find that, increasing the local frequency bounds, we gain significantly in computational accuracy while paying only slightly more in runtime and disk usage.

Table 4: Computational effort: ACMS with different numbers of subdomains

	Direct	ACMS/8	ACMS/16	ACMS/32	ACMS/64
# of Modes		498	495	475	470
Sys. time (min)	176.46	2.67	1.41	0.82	0.63
Disk usage (MB)	5,436.13	11,635.71	8,118.31	6,820.31	5,320.63

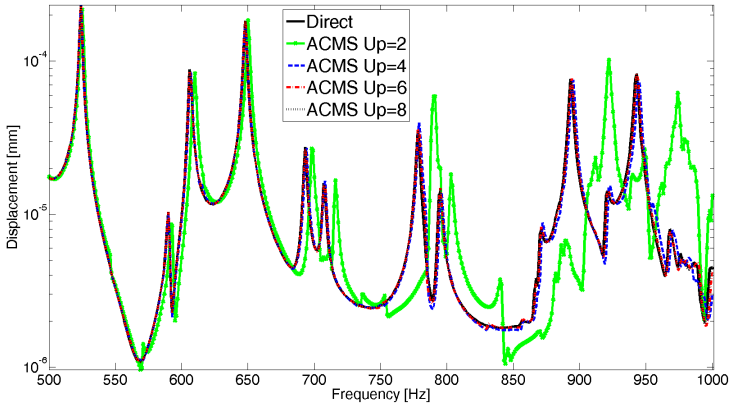

Figure 7: Domain decomposition: dependence on the upscale factor on subdomains

Summary

In conclusion of this subsection, we compare in Figure 8 and Table 6 the three reduction methods "MR", "CMS" and "AMLS"(ACMS) with the exact solution. Clearly, ACMS is superiour for this example under the combined criteria of reliability and efficiency. It is remarkable that all reliable setups of the reduction methods use about the same number of modes. All reduction methods require significantly less system time than the direct method. The disk usage is minimal for the direct method. The external CMS requires the least disk space of the reduction methods. It should be pointed out, however, that all ACMS computations are performed within the computational run itself, and the gain - both in time and disk space - from the internal CMS is remarkable. For this computational example, the optimal combination of accuracy and efficiency is achieved with ACMS, using a large number of subdomains with increased upscaling on the finest level.

It should be underlined once more that these conclusions are problem-dependent. The

Table 5: Computational effort: ACMS, varied modal upscaling on subdomains

	Direct	ACMS/2	ACMS/4	ACMS/6	ACMS/8
# of Modes		469	508	511	514
Sys. time (min)	176.46	0.62	0.89	1.07	1.14
Disk usage (MB)	5,436.13	5,320.63	6,340.50	7,481.94	7,055.69

relative differences in performance are significantly influenced by the modal density of the structure and the frequency band of excitations. Also we have not tested residual vectors in this part of our investigation.

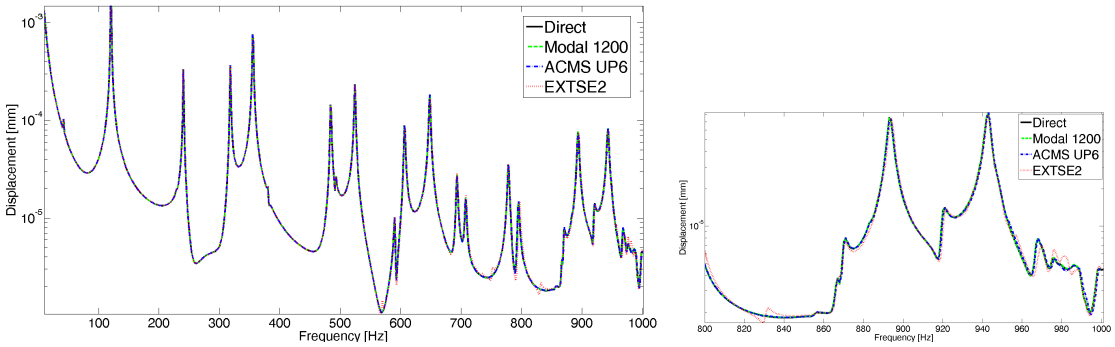

Figure 8: FRF: direct solution vs. reduction methods

Table 6: Computational effort: Direct solution vs. reduction methods

	Direct	Modal/1.2KHz	CMS/ext.	ACMS/6
# of Modes		517	515	511
Sys. time (min)	176.46	6.58	2.50	1.07
Disk usage (MB)	5,436.13	9,316.03	5,998.47	7,481.94

4.2 Large-scale model

The second series of tests was performed on the FE-model of several fuselage sections; see the sketch in Figure 9. The model size is about 2m nodal DOFs. The dynamic load is applied to the rear part of the structure.

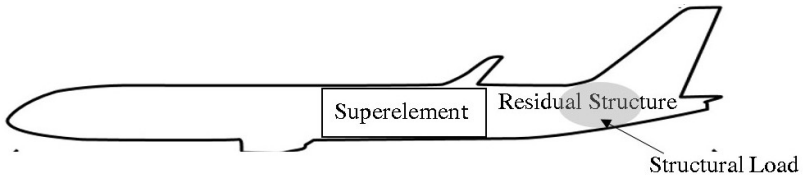

Figure 9: Sketch of the large-scale model

Computational Setup

The FRF is computed in seven bands, containing five single frequencies each. The root-mean-square of the normal velocities is computed over each band in every structural

node. Then the standard logarithmic dB scaling is applied. The results of the direct solution are again used as reference. The error is calculated as a difference of dB levels. We have used the percentile measure $50\%ile$[1] as the spatial medium of the errors over all measuring points. The reference solution is compared to ACMS and CMS ("external"). We evaluate the sensitivity of the reduction approach to computational parameters. In particular, we are interested in the impact of residual vectors on the performance of the reduction methods. The computational effort is measured by the four parameters System time (Time), Maximal Memory (MaxMem), Maixmal Disk Space (MaxDisk), I/O Transfer (I/O). The MaxMem values point to the usage of the computer's working memory, while the MaxDisk parameter indicates the disk space used by the particular job. The I/O parameter is an indicator of data transfer to scratch files.

ACMS

Local Frequency Limits (Upscale Factors): Starting from our conclusions for the medium-scale investigations, we first look at the influence of the upscaling on the subdomains. All computations have been carried out with ACMS, using the same maximal number N=256 of subdomains on the finest level and varying the upscale factor on the subdomains. The (global) frequency limit of modal analysis exceeds the maximal driving frequency by about 25% ($\omega_{\max} = 1.23\Omega_{\max}$). As can be seen from Figure 10, the upscaling parameter plays a minor role for the large-scale case. Note from Table 7 that the number of modes does not change significantly with the increase of the local frequency levels.

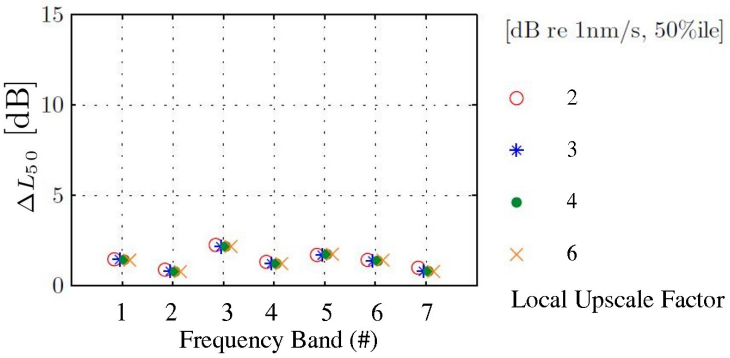

Figure 10: Computational results: Influence of the upscale factors

Global Frequency Limit: In Figure 11 and Table 8 we display the results obtained with different global frequency limits. The upper frequency $\omega_{\max}$ was increased to almost twice the maximal driving frequency. Again the number of subdomains is $N = 256$ and

[1]The $50\%ile$ measure indicates a statistical medium below which 50% of all observations fall. [17]

Table 7: Computational effort: Influence of the upscale factors

Measure/ Method		Upscale factor			
	Direct	2	3	4	6
# of Modes	-	8,110	8,217	8,247	8,266
Time (%)	100	23	29	37	53
MaxMem (%)	100	263	393	435	393
MaxDisk (%)	100	306	317	326	341
I/O	100	85	106	141	192

the local upscale factor has been set to 3 in all computations. Raising the global frequency limit has a larger influence on the results than the increase of the local upper limits via the upscale factor. The drop in the average error is most significant between $\alpha = 1.33$ and $\alpha = 1.72$. Note that this is correlated with the increase of the modal basis dimension. However, the quality gain comes with a higher computational cost.

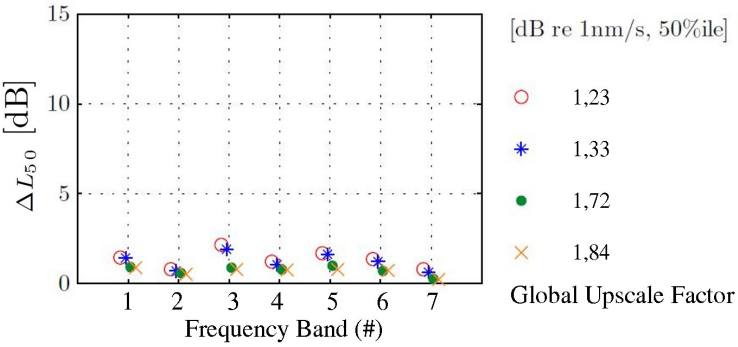

Figure 11: Computational results: Influence of the upper frequency $\omega_{\max} = \alpha\Omega_{\max}$.

Table 8: Computational effort: Influence of the upper frequency in modal analysis

Measure/ Method		Factor α			
	Direct	1.23	1.33	1.72	1.84
# of Modes	-	8,217	9,396	14,697	16,402
Time (%)	100	29	36	54	142
MaxMem (%)	100	393	393	479	545
MaxDisk (%)	100	317	356	537	595
I/O	100	106	126	194	213

Residual Vectors: We have seen that the increase of the modal basis leads to a decrease of the computational error, but also to a significant increase in computational cost. From

a theoretical viewpoint, it should be more efficient to represent the residual space by residual vectors than be additional eigenvectors. We therefore return to the variation of upscaling factors but now also include basis enrichment by residual vectors. Again the number of subdomains is $N = 256$, and the global frequency limit is set to the minimal $\omega_{\max} = 1.23\Omega_{\max}$ in all computations. The results are displayed in Figure 12 and the computational effort is reported in Table 9.

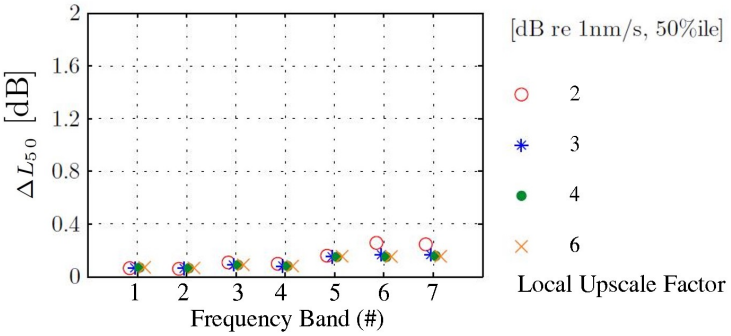

Figure 12: Computational results: Influence of residual vectors.

Table 9: Computational effort: Influence of residual vectors.

Measure/ Method		Upscale Factor			
	Direct	2	3	4	6
# of Modes	-	8,147	8,228	8,252	8,265
# of ResVec	-	+230	+224	+224	+224
Time (%)	100	27	33	44	63
MaxMem (%)	100	349	393	512	393
MaxDisk (%)	100	316	326	334	370
I/O	100	90	119	147	198

Clearly the quality of computational results is increased significantly by the basis enrichment, while the additional cost for the calculation and inclusion of residual vectors is minor (compare with the corresponding rows in Table 7, and note the different scaling of the y-axis in Figure 12).

The residual vectors have in this case a significant effect on the spatial distribution of the computational error. If the basis reduction is performed without residual vectors, the error is most pronounced in the rear part of the fuselage, as can be seen from Figure 13. Recall (see Fig. 9) that this is where the structural load is applied. This local effect is not observed in the calculations with residual vectors. A typical spatial distribution of the errors is shown in Figure 14. Recall that the residual vectors are computed from the

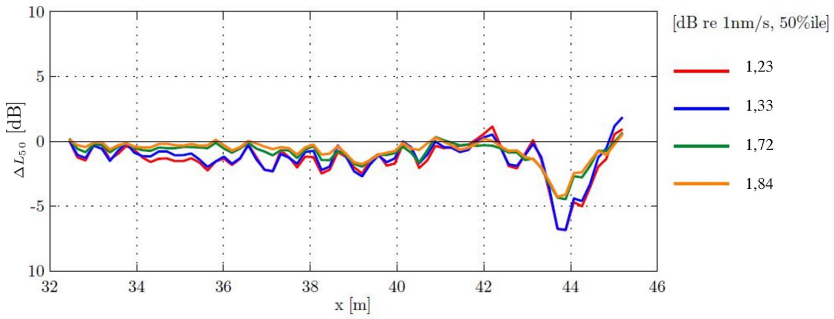

Figure 13: Computational error in longitudinal direction, w/o residual vectors, upscale factor 3, different frequency limits.

so-called static mode shapes. Unlike the eigenmodes, the static mode shapes depend on the exterior load and thus directly reflect the local force concentrations.

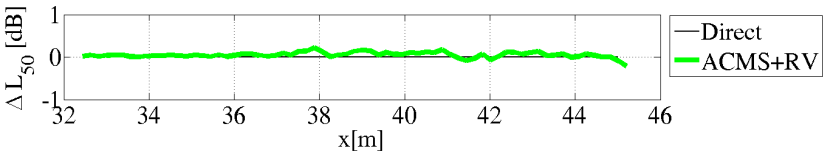

Figure 14: Computational error in longitudinal direction, with residual vectors, upscale factor 3, frequency limit $\alpha = 1.23$.

CMS (External Superelement)

We have also compared ACMS with CMS. Since it is clear that the internal CMS approach cannot compete with ACMS we have tested only the external approach. The two front sections of the fuselage were precalculated and used as an external superelement in the FR analysis. We have tested several variants with different modal upscaling α in the superelement. The results are compared with the optimal ACMS variant ($\alpha = 1.23$ and upscale factor 3) in Table 10. Residual vectors were included both in ACMS and in CMS. The spatial distribution of the computational error is shown in Figure 15.

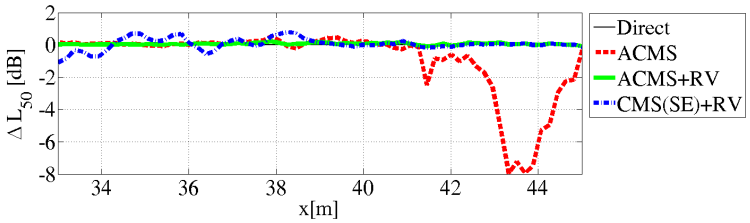

Figure 15: Computational results: Influence of residual vectors.

All reduced basis approaches need less run time than the direct method. The ACMS calculations were the fastest. The direct method needs the least disk space. The ACMS run needed less disk space than all CMS variants.

Table 10: Computational effort: ACMS vs. External Superelements

Measure/ Method			Ext. SE, Factor α		
	Direct	ACMS	1,22	1,84	2,45
# of Modes	-	8228	8268	8285	8286
# of ResVec	-	+224	+84	+84	+84
Time (%)	100	25	30	38	42
MaxMem (%)	100	393	393	393	393
MaxDisk (%)	100	327	327	536	768
I/O	100	105	41	48	49

Summary

We summarize the comparison of computational effort in Table 11. This final comparison, together with the error plots in Figure 15, underlines again the importance of AMLS for the computational efficiency, and of the basis enrichment by residual vectors for reliability and quality of the frequency response simulation.

Table 11: Computational effort: Direct method vs. ACMS (with and without ResVec) vs. Superelements (SE, with ResVec). All ACMS and SE calculations with $\alpha = 1.23$ and upscale factor 3.

	Direct	ACMS	ACMS +ResVec	SE +ResVec
# of Modes	-	8217	8228	8286
# of ResVec	-		+224	+84
Time (%)	100	29	33	39
MaxMem (%)	100	171	171	171
MaxDisk (%)	100	322	330	331
I/O	100	105	119	46

5 Conclusions

Reduced-order methods are frequently used for frequency response calculations in industrial applications. The dimensional reduction is achieved by a basis transformation $\mathbf{T}$ that projects the FRA to a low-order subspace. We review several methods of constructing the transformation operator, including modal reduction, domain decomposition, and Krylov-subspace methods. We then discuss the efficiency and reliability of these methods

from a theoretical viewpoint. Here we point out that the combination of eigenvectors with residual vectors accounts for both the inherent dynamics of the structure and the particular dynamical effects of the external loading. We have tested several reduction methods on FE-models for thin-walled structures of different size, and in different frequency bands. We use the direct solution as reference and compare the results and the computational effort of Modal Reduction, Component Modal Synthesis (CMS), and Automated Multilevel Substructuring (AMLS). The tests have shown a superior performance of AMLS, combined with basis enrichment by residual vectors.

REFERENCES

[1] Bai, Z., Krylov subspace techniques for reduced-order modeling of large-scale dynamical systems, *Appl. Num. Math.* 43 (2002), 9–44

[2] Bennighof, J., An adaptive multi-level substructuring method for efficient modeling of complex structures, *33. AIAA/ASME/Structural Dynamics and Materials Conference*, pp. 1631–1639, Dallas, TX, 1992

[3] Bennighof, J. and Lehoucq, R., An Automated Multilevel Substructuring Method for Eigenspace Computation in Linear Elastodynamics, *SIAM J. Scient. Comp.* 25, 6, pp. 2084–2106, 2004

[4] Bonin, Th., Faßbender, H., Soppa, A., and Zaeh, M., A fully adaptive rational global Arnoldi method for the model-order reduction of second-order MIMO systems arising in structural dynamics, https://www.tu-braunschweig.de/icm/numerik/personal/fassbender/papers (date of access: 2014.03.10)

[5] Büchner, B. and Möllenhoff, R., Anwendbarkeit der Component Mode Synthesis in akustischen Fragestellungen, Technical Report, Hamburg, 2012

[6] Carney, K.S., Abdallah, A.A., and Hucklebridge, A.A., Implementation of the block-Krylov boundary flexibility method of component synthesis. Kelly S.Carney, http://web.mscsoftware.com/support/library/conf/wuc93/p02693.pdf (date of access: 2014.3.10)

[7] Chargin, M., Description of CDH/AMLS, Restrictions/Limitations, Ingolstadt, CDH, 2002

[8] Craig, R. B., Coupling of substructures for dynamic analysis, *AIAA Journal* 7 , pp. 1313-1319, 1968

[9] Dickens, J., A critique of mode acceleration and modal truncation augmentation methods for modal response analysis. *Comp.Struct.* 1997 (6), pp. 985-998.

[10] Gao, W., Li, X. S., and Yang, An Implementation and Evaluation of the AMLS Method for Sparse Eigenvalue Problems. ACM Transactions on Mathematical Software 34, pp. 1–28, 2008

[11] G. H. Golub, C.F. van Loan, *Matrix Computations*, 3d Ed., John Hopkins, Baltimore 1996

[12] Guyan, R., Reduction of stiffness and mass matrices. *AIAA Journal* 3, 1965, p. 380

[13] J.S. Han, Efficient frequency response and its direct sensitivity analyses for large-size finite element models using Krylov subspace-based model order reduction, *J. Mech. Sc. Techn.* 26(4), 2012, 1115–1126

[14] Hurty, W., Dynamic analysis of structural systems using component modes. *AIAA Journal* 3, 1965, pp. 678–685.

[15] Kim, C.H. and Bennighof, J. K., Fast frequency response analysis of large-scale structures with non-proportional damping, *Int. J. Num. Methods Eng.*,69 (2007), 5, 978992

[16] Möllenhoff, R. (2012). Reduktionsverfahren für die vibroakustische Simulation von Flugzeugstrukturen mit der Finite-Elemente-Methode. Technical Report, UAS Hamburg, 2012

[17] Möser, M., *Messtechnik der Akustik*, Berlin, Springer, 2007

[18] Nour, O.B. and Clough, R. W., Dynamic analysis of structures using Lanczos coordinates, UC Berkeley, Center for Pure and Applied Mathematics, 1983

[19] Stammberger, M. and Voss, H., Automated multi-level sub-structuring for fluid-solid interaction problems. *Num. Lin. Alg. Appl.* 2011 (3), pp. 411–427.

[20] Wilson, E. A new method of dynamic analysis for linear and nonlinear systems, *Finite Elements Anal. Des.* 1985 (1), pp. 21–23.